



HAL
open science

The Use of Composite TiO₂/Activated Carbon Fibers as a Photocatalyst in a Sequential Adsorption/Photocatalysis Process for the Elimination of Ciprofloxacin

Thibaut Triquet, Claire Tendero, Laure Latapie, Romain Richard, Caroline Andriantsiferana

► To cite this version:

Thibaut Triquet, Claire Tendero, Laure Latapie, Romain Richard, Caroline Andriantsiferana. The Use of Composite TiO₂/Activated Carbon Fibers as a Photocatalyst in a Sequential Adsorption/Photocatalysis Process for the Elimination of Ciprofloxacin. *Catalysis Research*, 2022, 2 (1), pp.1-1. 10.21926/cr.2201007 . hal-03930724

HAL Id: hal-03930724

<https://hal.science/hal-03930724v1>

Submitted on 26 Apr 2023

HAL is a multi-disciplinary open access archive for the deposit and dissemination of scientific research documents, whether they are published or not. The documents may come from teaching and research institutions in France or abroad, or from public or private research centers.

L'archive ouverte pluridisciplinaire **HAL**, est destinée au dépôt et à la diffusion de documents scientifiques de niveau recherche, publiés ou non, émanant des établissements d'enseignement et de recherche français ou étrangers, des laboratoires publics ou privés.



Distributed under a Creative Commons Attribution 4.0 International License

Research Article

The Use of Composite TiO₂/Activated Carbon Fibers as a Photocatalyst in a Sequential Adsorption/Photocatalysis Process for the Elimination of Ciprofloxacin

Thibaut Triquet^{1,*}, Claire Tendero², Laure Latapie¹, Romain Richard¹, Caroline Andriantsiferana^{1,*}

1. Laboratoire de Génie Chimique, Université de Toulouse, CNRS, INPT, UPS, Toulouse, France; E-Mails: thibaut.triquet@univ-tlse3.fr; laure.latapie@univ-tlse3.fr; romain.richard@iut-tlse3.fr; caroline.andriantsiferana@iut-tlse3.fr
2. Centre Inter-universitaire de Recherche et d'Ingénierie des Matériaux, Université de Toulouse, CNRS, Toulouse, France; E-Mail: claire.tendero@toulouse-inp.fr

* **Correspondences:** Thibaut Triquet and Caroline Andriantsiferana; E-Mails: thibaut.triquet@univ-tlse3.fr; caroline.andriantsiferana@iut-tlse3.fr

Academic Editor: Youliang Cheng**Special Issue:** [Photocatalysis for Water and Wastewater Treatment](#)*Catalysis Research*

2022, volume 2, issue 1

doi:10.21926/cr.2201007

Received: January 20, 2022**Accepted:** March 06, 2022**Published:** March 15, 2022

Abstract

This work reports the performance of a sequential adsorption/photocatalysis process using activated carbon fibers with deposited TiO₂ for the elimination of the antibiotic ciprofloxacin (CIP) in water. A commercial activated carbon fiber (ACF10) was selected as the support, and a TiO₂ coating was synthesized using Metal Organic Chemical Vapor Deposition (MOCVD). Experiments were carried out using a photocatalytic reactor irradiated with monochromatic LEDs (365nm). Two different processes have been studied: adsorption/photolysis and adsorption/photocatalysis. The objective was to completely remove the CIP and to evaluate the efficiency of the treatment by following the formation/elimination of aromatic transformation products (ATPs), aliphatic acids, fluoride, and the TOC in the liquid phase. The adsorption kinetic of the CIP by ACF10 was rather slow (71% of CIP adsorbed by 24 h and total adsorption by 20 days). A good fit between the external diffusion limitation model and the



© 2022 by the author. This is an open access article distributed under the conditions of the [Creative Commons by Attribution License](#), which permits unrestricted use, distribution, and reproduction in any medium or format, provided the original work is correctly cited.

experimental curve ($k_{\text{ext}} = 0.0056 \text{ h}^{-1}$) showed an external transfer limitation due to a tight weave of fibers. For the adsorption/photolysis process, a significant decrease of the concentration was achieved (95% after 6 h of irradiation), but ten different ATPs were detected in the liquid phase. To eliminate CIP, 24 h of adsorption and 6 h of irradiation were then necessary, but most of the ATPs remained in solution (total treatment duration: 72 h). With ACF10-TiO₂, the same ATPs were present in solution and were eliminated after the 6 h irradiation step (total treatment duration: 30 h). At the end of the treatment, several non-toxic aliphatic acids were found to be present, showing the higher efficiency of this sequential process. The presence of a significant amount of fluorine in the liquid phase suggests some surface photochemical reactions of the adsorbed molecules (CIP and transformation products) and a partial regeneration of the composite material.

Keywords

Activated carbon fiber; photocatalysis; adsorption; ciprofloxacin; hybrid process; MOCVD; TiO₂

1. Introduction

Even if water is in abundance on Earth, preserving its purity in the natural environment is crucial for the future. Over the last few decades, many toxic molecules named micropollutants or endocrine disruptors were detected in the rivers and underground waters, with serious consequences for the environment [1-3]. Their occurrence in natural water sources is constantly increasing on a scale ranging from $\text{ng}\cdot\text{L}^{-1}$ to $\mu\text{g}\cdot\text{L}^{-1}$ due to anthropogenic activities [4]. Therefore, global and European legal limits have been lowered to reduce the environmental impacts of these micropollutants [5]. Conventional wastewater treatments (i.e., filtration, settling, biological processes, etc.) cannot totally eliminate these molecules, and additional treatments are therefore necessary. These techniques include advanced oxidation processes (AOP), separation processes (adsorption, stripping...), and biological processes (membrane bioreactor [6]). Among all of these techniques, two processes seem to be adequate for micropollutants removal: adsorption and AOP processes. Adsorption processes are some of the most efficient and economic processes [7], and removal rates close to 100% can be achieved [8, 9]. The most common adsorbent is activated carbon which can be found in three different forms (powder, granular, or fiber). Activated carbon is the most widely used adsorbent in the field of wastewater treatment because of its very good cost/efficiency ratio and its excellent adsorption capacity directly linked to its large specific surface [10, 11]. Activated carbon fibers (ACF), due to their small size (between 10 and 40 μm of diameter), have a much better pore volume/surface area ratio than other adsorbents [12]. In addition, these fibers are mostly microporous materials. As the size of the micropollutants is generally small (0.1 - 3 nm), the use of this type of adsorbent allows fast kinetics since the internal transfer is more easily achieved (adsorbate size < pore size) [13]. ACFs have proven to be effective for several micropollutants such as methylene blue [14], bisphenol [15, 16], diclofenac [17], and ciprofloxacin [18]. The main drawback of the adsorption process is that the molecules are not degraded. Thus, they remain fixed on the adsorbent, and it is, therefore, necessary to regularly change or regenerate the adsorbent *in*

situ (often a very difficult and sometimes almost impossible operation). Advanced oxidation processes (AOP) include many different processes: Fenton reactions, anodic oxidation, oxidation [19], electro-Fenton, photocatalysis [20, 21], corona discharge [22], catalytic, or UV, or H₂O₂ coupled with ozonation [23], sonochemical reactions [24] etc. AOPs have been extensively studied, and their excellent ability to remove and degrade micropollutants has been demonstrated by many authors [25]. For heterogeneous photocatalysis, the catalyst is a solid semiconductor activated by light radiation. The photocatalyst absorbs light to create free electrons (e⁻) and holes (h⁺), allowing the production of extremely reactive hydroxyl radicals (OH^{*}) [26]. Photocatalysis has proven its efficiency for the elimination of many different micropollutants such as, for example, ciprofloxacin [27], tylosin [28], and triazole [29]. Titanium dioxide (TiO₂) is the most widely used photocatalyst. However, usually available in powder form, TiO₂ must be removed at the end of the process by an expensive separation step. Moreover, there is a suspected risk of chronic intestinal inflammation and carcinogenesis from TiO₂ use due to the size of the particles (mainly nanoparticles) [30]. Consequently, most authors propose the use of a TiO₂ coating on multiple materials: glass [31], metal [32], adsorbent [33, 34], membrane [35], etc. When the catalyst is deposited on an adsorbent, the objective is to combine adsorption and an oxidation technique to degrade the adsorbed molecules and thus regenerate the adsorbent [36]. Therefore, the drawbacks of the two processes (separation step for photocatalysis and saturation of the adsorbent for adsorption) can be overcome. These hybrid processes can be implemented either sequentially or simultaneously. Supported TiO₂ has already been studied and showed excellent results [37]. However, ACF/photocatalyst composite materials are little studied in the field of wastewater treatment [38]. In this category, different types of fibers can be found, such as commercial fabrics [12, 39, 40], fibers made from natural resources such as coconut [41], carbon nanotubes [42, 43], and graphene-like materials [44]. For commercial activated carbon fibers, studies are often focused on the materials (i.e., on the synthesis or deposition of the coating and its characterization). In general, these studies follow the evolution of the concentration in the liquid over time for simultaneous or sequential implementation [45]; most report the reuse of the material over several cycles [46, 47]. In general, the conclusion is that the catalytic material is highly efficient since most authors report elimination rates higher than 95% [48, 49]. However, the performance may decrease after several reuses. Few authors are interested in the transformation products (TP) formed and the monitoring of their concentrations over time, and most authors choose global measures such as total organic carbon (TOC), chemical oxygen demand (COD), or biological oxygen demand (BOD).

For this study, the antibiotic Ciprofloxacin has been selected as the target molecule. This fluoroquinolone is representative of the recalcitrant micropollutants found in municipal wastewater treatment plants. A sequential process has been selected combining adsorption and photocatalysis. To carry out this coupling process, a hybrid material was synthesized: a TiO₂ coating deposited on commercial activated carbon fibers using the Metal Organic Chemical Vapor Deposition (MOCVD) technique. Activated carbon fibers were chosen to concentrate as much as possible the target molecules close to the TiO₂ coating and to be able to degrade them afterward by photocatalysis. To evaluate the performances of this process, the liquid phase was completely analyzed by following the CIP concentration, the production and the elimination of transformation products, the concentration of fluoride, and TOC. The objective of this study was to answer the following questions: does this kind of treatment provide better performance than a single adsorption process? Does this process limit the amount of TPs formed? Does it regenerate the catalytic material *in situ*?

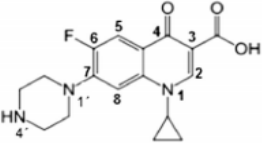
The novelty of this work is to (i) follow all the molecules that are produced and degraded during an adsorption/photocatalysis coupling and (ii) highlight and clearly demonstrate the potential photocatalytic activity of the composite material. Finally, the durability of TiO₂ coating is also investigated to make sure that it remains on the ACF fibers and is not dispersed in the treated water.

2. Materials and Methods

2.1 Chemicals

The target molecule for this study was ciprofloxacin, available at high analytical grade (CIP, 98% purity). All of its physico-chemical properties are presented in Table 1. Titanium tetraisopropoxide (TTIP, 99.999%) was used as the source of titanium for the coating of the ACF. Formic acid, CH₂O₂ (formic acid, >99% purity), and acetonitrile (suitable for HPLC, gradient grade, ≥99.9%) were used for liquid analysis. Each chemical product was purchased from Sigma Aldrich.

Table 1 Chemical and physical properties of CIP.

Molecule	Formula	Molar (g.mol ⁻¹)	Weight	pK _a [50]	Solubility at 25 °C [51]
	C ₁₇ H ₁₈ FN ₃ O ₃	331.35		3.64 (N1); 5.05 (N1'); 6.95 (OH); 8.95 (N4')	75 ±10 mg.L ⁻¹ in water 150 ±5 mg.L ⁻¹ in acetone 25 g.L ⁻¹ in acidic water (pH = 3)

2.2 Activated Carbon Fibers

The Activated Carbon Fibers (ACFs) product used for this study (ACF10) was supplied by KYNOL (Osaka, Japan). The different commercial characteristics of ACF10 are listed in Table 2.

Table 2 Supplier characteristics of the selected activated carbon fibers.

Supplier	KYNOL (Japan)
ACF	ACF 10
Supplier references	ACC-5092-10
Precursor	Novoid Fiber
Fiber diameter (μm)	10
Fabric thickness (mm)	0.66
BET specific surface (m ² .g ⁻¹)	1200
Adsorption I ₂ (mg.g ⁻¹)	1300
Pore volume (cm ³ .g ⁻¹)	0.35
Mean pore size (nm)	0.8
Weight (g.m ⁻²)	205

2.3 Deposition of TiO₂ Coating on ACF

Metal Organic Chemical Vapor Deposition (MOCVD) was used to synthesize the deposit. A horizontal tubular hot-wall reactor (heated at 500 °C) was used to grow the TiO₂ coating [52] with titanium tetraisopropoxide (TTIP, 99.999%, Sigma-Aldrich) as the precursor. This titanium source was thermoregulated in a bubbler at 50 °C and carried to the deposition zone under 99.9992% of pure nitrogen flow, which was used as both the carrier gas (25 cm³.min⁻¹) and the dilution gas (500 cm³.min⁻¹). The deposition was performed on each side of the ACF. To minimize the gradient of the coating thickness along the substrate, the deposit on each side was made twice, with 180° rotation of the ACF between the two steps. Each material was weighed before and after treatment to estimate the mass of TiO₂ coated on ACF.

2.4 Experimental Set-up

The experimental setup is shown in Figure 1. The batch process is carried out in a photo-reactor of 12 mL and a stirred storage tank of 100 mL. The circulation of the liquid is ensured by a peristaltic pump operating at a constant flow rate (200 mL.min⁻¹). The liquid is pumped from the storage tank through the photo-reactor equipped with a glass Pyrex® window (130 × 10 × 12 mm). The substrate is placed at the bottom of this reactor, and a monochromatic LED panel (365 nm) irradiates its upper face. The temperature inside the system was maintained at 25 °C (±1 °C) thanks to an aeration system.

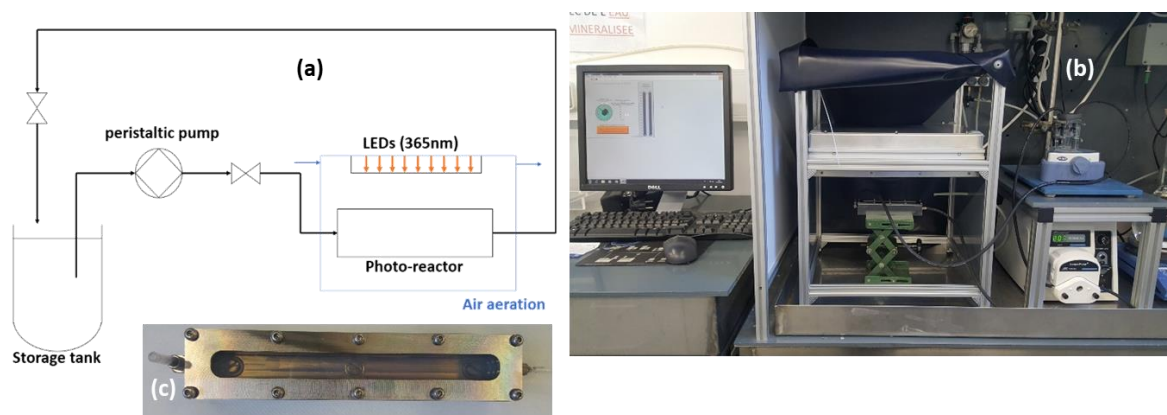


Figure 1 Experimental setup flow-diagram (a); experimental setup (b); photo-reactor (c) [37].

2.5 Experimental Protocols

Firstly, adsorption kinetics were measured without any TiO₂ coating on the surface, using the system shown in Figure 1. The size chosen for the ACF10 was equivalent to one-third of the total irradiated surface of the Pyrex®-glass window to have a compromise between a sufficient amount of adsorbent and a good-sized area of irradiated surface. The ACF10 piece, corresponding to 193 mg of ACF, was placed at the bottom of the photoreactor. The storage tank was filled with a 100 mL solution at 20 mg.L⁻¹ of CIP, and then the peristaltic pump was started. Samples were taken from the storage tank over a period of 72 h. Each liquid sample was filtered through a 0.45 μm Nylon filter before being analyzed. All experiments were performed three times.

For the adsorption/photolysis experiment, ACF10 (without TiO₂ coating) was used while a composite material was selected for the adsorption/photocatalysis process: ACF10 with deposited TiO₂ (labeled ACF10-TiO₂). Adsorption without UV was performed first for 24 h, followed by 6 h of uniform irradiation (Irradiance = 10 mW.cm⁻², λ = 365nm). Then, another 18 h of adsorption without UV followed. For adsorption/photolysis experiments alone, a further sequence of 6 h of irradiation and 18 h of adsorption were carried out. In practice, it was found that for adsorption/photolysis experiments, more irradiation and adsorption steps were necessary to eliminate the CIP. Liquid samples were taken in regular intervals from the storage tank, filtered through a 0.45 μm Nylon filter, and analyzed. Each experiment was carried out three times. At the end of the treatment, the composite material (ACF10-TiO₂) was characterized.

The irradiance was measured using a UVA light meter - RS232PC serial interface (Ultra-Violet Radiometer) purchased from Lutron (USA).

2.6 Liquid Analysis

Measurements of CIP concentration were carried out using a Thermo Accela HPLC-PDA from Shimadzu. For all analyses, a Phenomenex C18 column (2.6 μm, 100 mm x 3 mm) and a diode array UV detector (UV spectrum possible from 190 to 800 nm) were used. Two analytical methods were used (Table 3): one when only adsorption was involved (only CIP present) and one when irradiation was involved (CIP and transformation products present).

Table 3 Operating conditions for the HPLC-UV analysis.

Method	CIP alone (Adsorption)	CIP and transformation products
Mobile phase (A/B)	A: Acidified water with 0.1% formic acid (pH = 3) B: Acetonitrile	
Flow rate (mL.min ⁻¹)		0.3
Temperature (°C)		40
Detector wavelength (nm)		290
Volume injected (μL)		10
Solvent gradient: time-volume composition (A/B)	Isocratic method 0-7 min - 90/10	Gradient method 0 min - 90/10 0 - 7 min - 90/10 7 - 12 min - 90/10 12 - 19 min - 10/90 19 - 25 min - 10/90

Transformation products were identified by an HPLC-MS. A ThermoFisher UltiMate 3000 HPLC was used, coupled with an Orbitrap High-Resolution Mass Spectrometer (HRMS-Exactive) equipped with an Electrospray ionization source (ESI). The monochromatic wavelength was set to 280 nm for the UV detector, and a Gemini C18 column was used (3 μm, 100 mm x 2 mm). A standard mobile phase for HPLC was used (Table 3), and a gradient mode was selected. The flow rate was set to 0.2 mL.min⁻¹ at 40 °C. Initially, the mobile phase was maintained at 10/90 (v/v) for 2 min, then, to reach 90/10 (v/v), a linear increase was performed across 7 min and maintained for 8 min. Finally, the

composition of the mobile phase was decreased by a linear decrease across 3 min to reach the initial composition 10/90 (v/v) and then held for 6 min until the next injection. To identify the intermediates, both positive and negative ionization modes of the MS were used.

The amount of aliphatic acid and fluorine were determined by Ionic Chromatography (IC) using a Thermo Scientific ICS 5000+ ion chromatography with a conductimetric detector. An AS19 (4 μm , 2 \times 250 mm) anion column was used. The flow rate was maintained at 0.250 mL.min⁻¹ at 25 °C. KOH solution was used as the mobile phase, and a gradient method was employed. A concentration of 5 mmol.L⁻¹ of KOH is maintained for 10 min. To achieve 45 mmol.L⁻¹ of KOH, a linear increase was then carried out across 15 min, and the concentration was maintained for 10 min. Then, a decrease from 45 to 5 mmol.L⁻¹ was done by another linear decrease across 2 min.

A TOC-L (Total Organic Carbon Analyzer) from Shimadzu (Japan) was used for TOC measurements. The value of total carbon was firstly determined by a 20 μL injection, then the inorganic carbon was determined with a second injection of 50 μL with hydrochloric acid (0.1 mol.L⁻¹).

ICP measurements were carried out using ICP-AES (Ultima2, Horiba, Japan) to determine the quantity of titanium in the liquid phase at the end of the treatment. The power source was set at 1,100 W, with a continuous plasma gas flow rate of 12 L.min⁻¹, a cladding gas flow rate of 0.2 L.min⁻¹, and a pump speed of 15 tr.min⁻¹. A glass concentric nebulizer and a glass cyclone chamber were used for every analysis.

2.7 Solid Analysis

Scanning Electron Microscopy (SEM) observations were done with an LEO-435 VP-PGT scanning electron microscope to visualize the morphology of both raw and coated activated carbon fibers and an FEI Quanta450 for further analysis of the chemical composition. The crystalline structure was then investigated by X-Ray Diffraction (XRD) on a GI-XRD Bruker D8 instrument.

The tensile tests were carried out on the INSTRON 3367: the elongation of the fabric (mm) as a function of the tensile load (N) was monitored via the Bluehill acquisition software. The speed rate was set at 1 mm.min⁻¹, and each ACF tested had the same dimension (150 \times 20 \times 0.5 mm³) with 100 mm placed between the jaws. The tensile tests were performed to characterize both ACF materials (tensile strength, elasticity, Young's modulus).

To determine the BET specific surface area, measurements were carried out with the Autosorb-I_Quantachrome BELMaster, a volumetric gas adsorption device. Before each measurement, the sample was degassed under vacuum at 200 °C for 2 h. For the determination of the BET specific surface area, the BET method was used from the adsorption and desorption isotherms of nitrogen (N₂) at - 196 °C. This method was proposed in 1938 by Brunauer, Emmett, and Teller and is based on the multilayer adsorption theory [53].

The pore size distribution was obtained with the same measuring device as that used for the determination of the BET specific surface area, but via a different method: the NLDFT method (Non-Localized Density Functional Theory). The NLDFT method was coupled with the "slit-shaped" geometric pore model, which has been adapted for granular or fiber-type activated carbon materials [54, 55].

3. Results

3.1 Adsorption

3.1.1 Characterization of the ACF

The physical properties of ACF10 have been measured. The BET surface area was $926 \text{ m}^2.\text{g}^{-1}$, a rather low value compared to that of other ACF of up to $3000 \text{ m}^2.\text{g}^{-1}$ [12]. The total volume was $0.38 \text{ cm}^3.\text{g}^{-1}$, and the microporous volume was $0.35 \text{ cm}^3.\text{g}^{-1}$: 92% of the pores correspond to micropores. Figure 2 shows the pore size distribution of the adsorbent with two significant peaks in the range of microporous sizes. These results confirmed the microporous nature of ACF10.

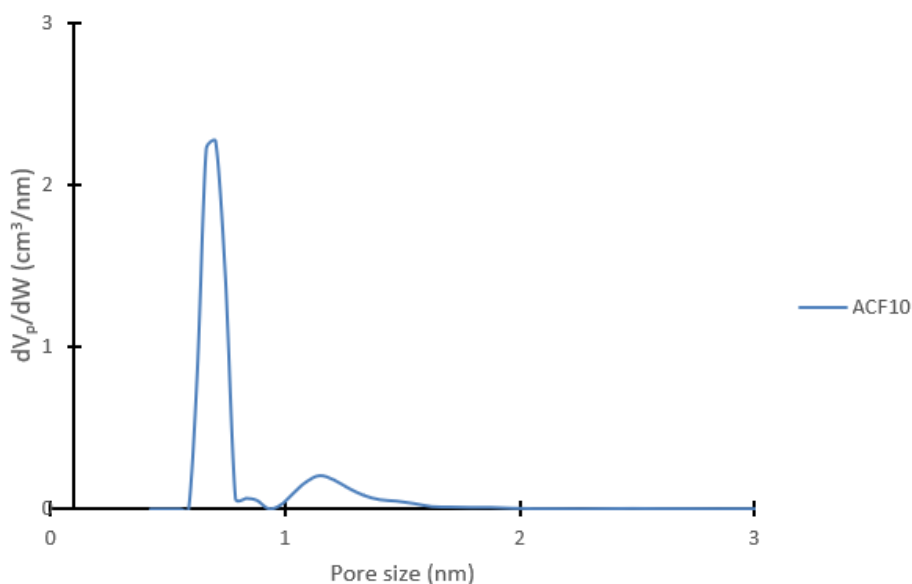


Figure 2 Pore size distribution of ACF10.

The macroscopic structure and weaving pattern were also investigated (see Figure 3). ACF10 shows particularly strong longitudinal lines (probably the warp direction). Scanning electron microscopy (SEM) confirms this first observation and suggests that ACF10 has a tight weave. Finally, the cross-section shows a compact fiber bundle.

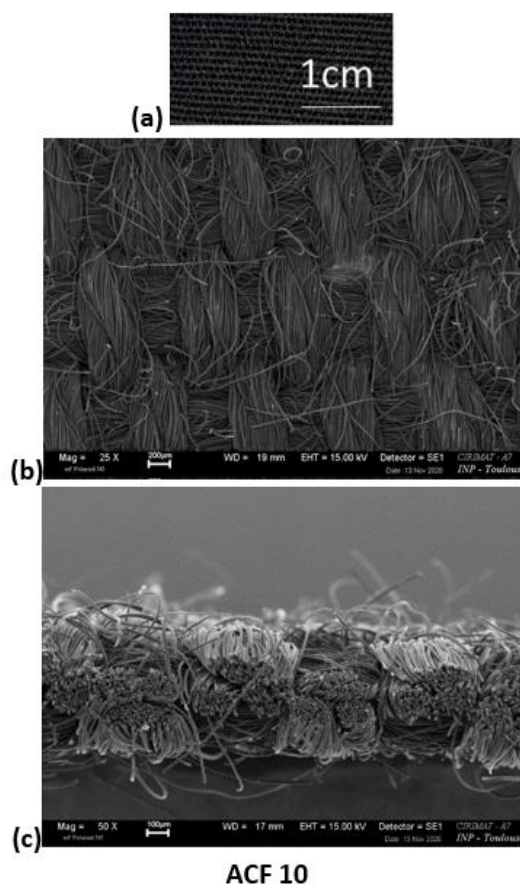


Figure 3 Optical (a) and Scanning Electron Microscopy images of ACF10 at different scales. (b): top view, (c): cross-section.

Finally, ACF10 was tested under tensile stress to determine whether its resistance and elasticity were affected or not by the thermal treatment (500 °C during 2-3 h) used during the TiO₂ deposition step. All results are presented in Table 4. The heat treatment results in a 25% reduction of Young's modulus E and a slight decrease of the ultimate tensile strength and the failure strain. After this treatment, the ACF10 fabric was thus considered to remain resistant and rigid.

Table 4 Young's modulus E , ultimate tensile strength σ_{\max} , and failure strain A_f of ACF10 with and without (reference) heat treatment (500 °C).

	Reference	Heat treatment
E(MPa)	640 ±40	480 ±40
σ_{\max} (MPa)	8 ±1	7.5 ±0.7
A_f %	3.5 ±0.1	3.8 ±0.1

3.1.2 Kinetics of CIP Adsorption on the ACF

In this study, an initial concentration (20 mg.L⁻¹), which is higher than the value reported in the outlet of domestic wastewater treatment plants (100 ng.L⁻¹), has been chosen [4, 56-58]. This choice is justified by the strong adsorption capacities of ACF - with lower initial concentrations, all the

molecules would have been adsorbed, and nothing would have remained in the liquid phase after the different treatment steps. Figure 4 shows the adsorption kinetics for CIP with ACF10 (experimental results and modeled kinetics). The blank curve corresponds to experiments without ACF10 - around 10% of CIP can be adsorbed in the experimental device corresponding to the part of CIP retained in the system (tubes, pump, etc.). The adsorption kinetics obtained with ACF10 is rather slow: total adsorption is reached after 480 h (20 days), and only 71% is adsorbed after 24 h.

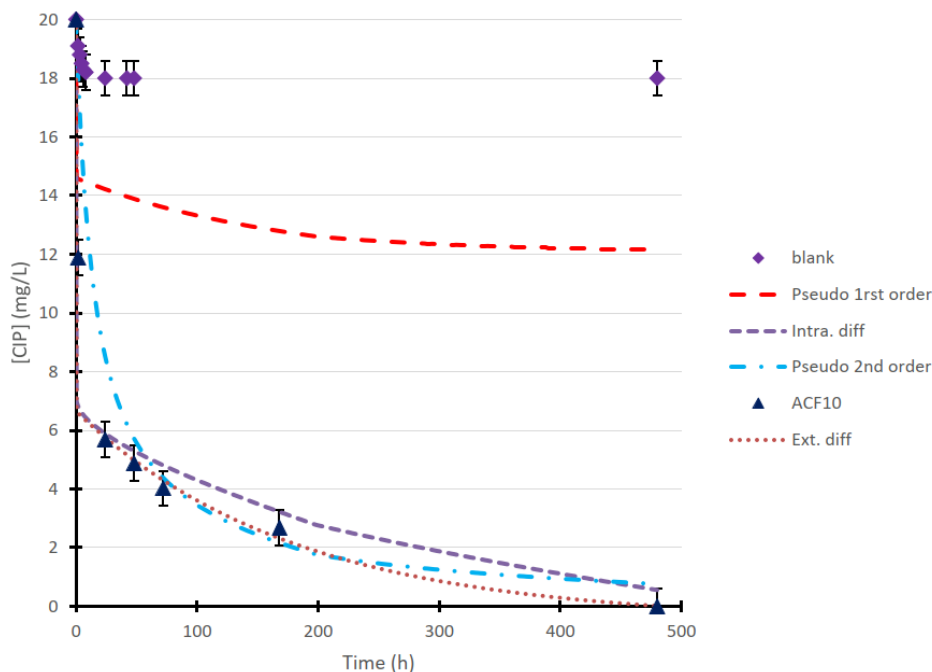


Figure 4 Adsorption kinetics of CIP on ACF10 ($C_0 = 20 \text{ mg}\cdot\text{L}^{-1}$; $V = 100 \text{ mL}$; $m_{\text{ACF10}} = 193 \text{ mg}$; $T = 25 \pm 2 \text{ }^\circ\text{C}$).

In addition, several models have been used to represent the adsorption kinetics:

- External diffusion model: in this case, the external diffusion of CIP to the surface of ACF10 is the limitation step. Then the kinetics can be described with the conventional external diffusion model [59, 60]:

$$-\frac{dC_t}{dt} = k_{ext}(C_t - C_e)$$

Where C_t is the concentration of CIP in the liquid phase, t the adsorption time, C_e the concentration of CIP at the equilibrium, and k_{ext} the kinetic constant. Thus, this equation can easily be linearized as follows:

$$\ln \left[\frac{C_0 - C_e}{C_t - C_e} \right] = k_{ext} \cdot t$$

A simple plot of $\ln [C_0 - C_e] / (C_t - C_e)$ versus reaction time will allow the determination of the kinetic constant k_{ext} .

- Intra-particle diffusion model: in this case, the limitation step is the diffusion of CIP inside the pore of ACF10. This kinetics can be described by the following model [61]:

$$q_t = k_{intra}t^{0.5} + A$$

Where q_t the actual quantity adsorbed on ACF, k_{intra} the kinetic constant, t the adsorption time, and A a constant.

- pseudo first-order model. This model is generally applicable for short adsorption kinetics (about 30 min). The partial order is 1 with respect to the free site concentration and 0 with respect to the solute in solution. This model neglects desorption by coupling the adsorption and desorption constants into one [62]:

$$\frac{dq}{dt} = k_1(q_e - q_t)$$

Where q_t the actual quantity adsorbed on ACF, q_e the quantity adsorbed on the ACF at the equilibrium, k_1 the pseudo first-order kinetic constant. This equation can be linearized:

$$\ln(q_e - q_t) = \ln(q_e) - k_1t$$

- pseudo second-order. A more robust model than the pseudo first-order. This model can be considered as a simplified case of a case where the adsorption kinetics is managed by the surface reaction rate [63, 64]:

$$\frac{dq}{dt} = k_2(q_e - q_t)^2$$

Where q_t is the actual quantity adsorbed on the ACF, q_e the quantity adsorbed on the ACF at the equilibrium, and k_2 the pseudo second-order kinetic constant. This equation can be linearized as follows:

$$\frac{t}{q} = \frac{1}{k_2q_e^2} + \frac{1}{q_e}t$$

All four models were used to represent the adsorption kinetics of CIP on ACF10, and the different constants obtained are presented in Table 5.

Table 5 Coefficients of the kinetics of CIP adsorption on ACF10 for the different kinetic models.

Limitation							
External diffusion	Intra-particle diffusion			Pseudo first order		Pseudo second order	
$k_{ext} (h^{-1})$	0.0056	$k_{intra} (mg.g^{-1}.h^{-0.5})$	0.1227	$q_e (mg.g^{-1})$	3.77	$q_e (mg.g^{-1})$	9.48
		$A (mg.g^{-1})$	6.602	$k_1 (h^{-1})$	0.0062	$k_2 (g.mg^{-1}.h^{-1})$	0.0071
R^2	0.9955	R^2	0.9949	R^2	0.8392	R^2	0.9988

The results show that the pseudo first-order model is not suitable for CIP adsorption on ACF10 as confirmed by the theoretical curve calculated by using the specific pseudo first-order parameters. However, even if excellent R^2 values were found with the other models, only the external diffusion limitation model presents a very good fit between the experimental and model curves (Figure 4). This limitation of external diffusion was due to the tight weave of ACF10.

3.2 Coupling Process

3.2.1 The Adsorption and Photolysis Coupling Process

Kinetics of CIP Elimination. As CIP can be degraded by photolysis, it is necessary to study the coupling of adsorption and photolysis (degradation under UV irradiation) before using the material with TiO_2 coating to investigate the adsorption/photocatalysis coupling process [37]. For this study, the same volume of CIP solution (20 mg.L^{-1}) has been used during the following steps of the process:

- First adsorption step: 24 h (UV off)
- First irradiation step: 6 h (UV on)
- Second adsorption step: 18 h (UV off)
- Second irradiation step: 6 h (UV on)
- Final adsorption step: 18 h (UV off)

Figure 5 shows the CIP elimination kinetics during the complete process. For comparison, the kinetics of the adsorption on ACF across 72 h has been added to the same figure.

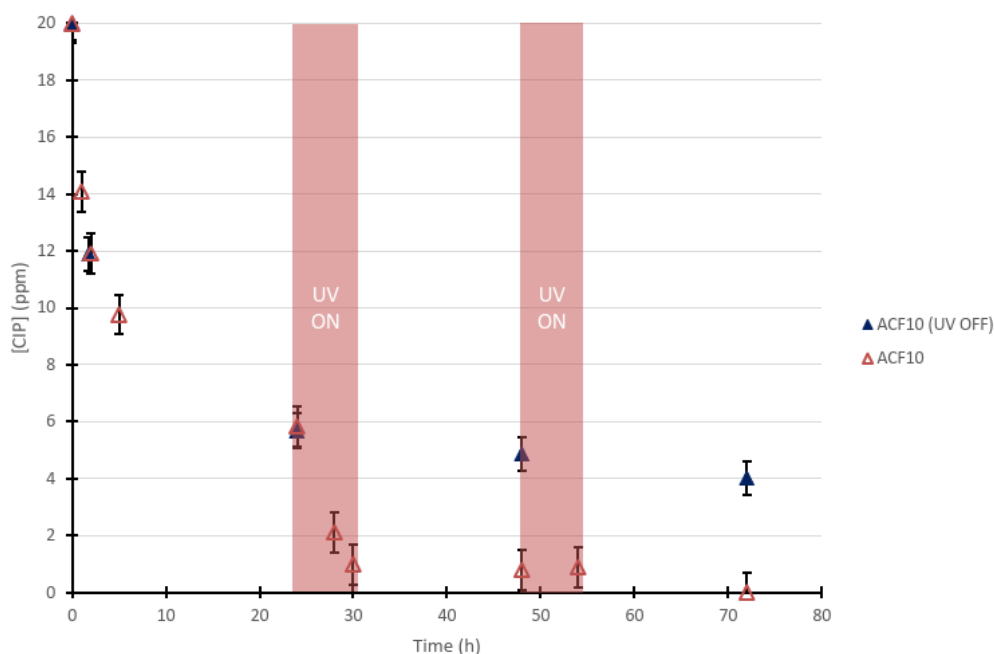


Figure 5 Elimination of ciprofloxacin by coupling adsorption and photolysis (UV alone) for both ACFs ($C_0 = 20 \text{ mg.L}^{-1}$; $V = 100 \text{ mL}$; $m_{KIP1200} = 123 \text{ mg}$; $m_{ACF10} = 193 \text{ mg}$; $I = 10 \text{ mW.cm}^{-2}$; $T = 25 \text{ }^\circ\text{C}$).

Only 71% of CIP was adsorbed by using ACF10 after 24 h of adsorption, and only 80% after 70 h. For the sequential process, after the first phase of UV-irradiation, 95% of the CIP had been removed. This irradiation allowed the elimination of CIP in solution by photolysis and adsorption (simultaneous processes). This behavior has already been observed: faster methylene blue removal when photolysis and adsorption were coupled in a simultaneous process has been reported [65]. After the second adsorption step, the CIP amount adsorbed is of the order of the magnitude of the error: this step did not remove any CIP molecules. During the first UV-irradiation, transformation products were formed; thus, competitive adsorption between these molecules and CIP could take place, which would lead to slower adsorption kinetics of CIP. During the second irradiation phase, very little amount of CIP degrades: all the transformation products present in the liquid compete with CIP for photo-degradation. Finally, even if CIP is eliminated with the adsorption/photolysis sequential process, the duration of the treatment is too long to be industrially interesting (70 h).

Aromatic Transformation Products. Every aromatic transformation product (A, B, C...) obtained during the photolysis of CIP was identified and their evolution investigated (each letter corresponds to one aromatic transformation product or isomer product - Table 6) [37].

Table 6 Aromatic transformation products after CIP photocatalytic degradation.

Molecule	Molecule structure [27]	Retention time (min)	Molecule	Molecule structure [27]	Retention time (min)
A C ₁₇ H ₁₉ N ₃ O ₄		3.0	F C ₁₆ H ₁₆ FN ₃ O ₄		4.6
B C ₁₅ H ₁₇ N ₃ O ₃		3.1	G C ₁₄ H ₁₁ FN ₂ O ₄		4.72
C C ₁₅ H ₁₆ FN ₃ O ₃		3.3	H C ₁₃ H ₁₁ FN ₂ O ₃		4.98
D C ₁₇ H ₁₆ FN ₃ O ₅		4.06	I C ₁₇ H ₁₇ N ₃ O ₅		3.9
E C ₁₃ H ₁₂ N ₂ O ₃		4.37	J C ₁₆ H ₁₇ N ₃ O ₄		4.3

Many ATPs were detected. The evolution of their concentration is shown in Figure 6. During the first phase of UV irradiation, most of the ATPs were produced, and some of them had started to be

degraded. However, 6 h of irradiation is not sufficient for their total elimination since photolysis is a slow and selective reaction [66]. The second adsorption step showed adsorption of ATPs, which could explain the slower adsorption kinetics of CIP in Figure 5. After two UV-irradiation steps and three adsorption steps, some ATPs remained in the liquid phase.

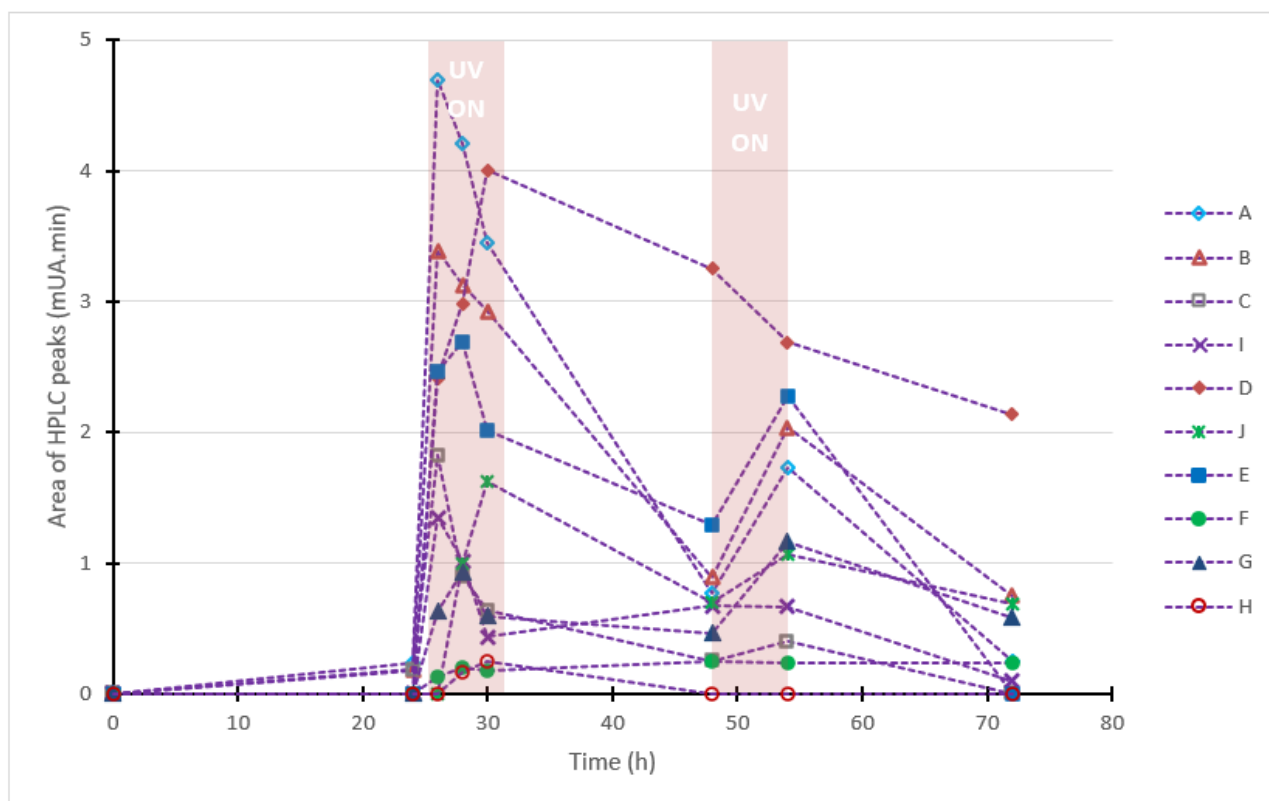


Figure 6 Evolution of the aromatic transformation products during the combined adsorption/photolysis process with ACF10.

Mineralization and Efficiency. For CIP, as shown by Triquet et al. [37], further refractory ultimate transformation products could be present such as aliphatic acids (HCOO^- and $\text{C}_2\text{O}_4^{2-}$) and even the fluoride ion F^- . These transformation products were searched for in the solution, but only fluoride F^- was detected and quantified.

Considering only the CIP present in the solution at the end of the first adsorption step (5.82 mg.L^{-1}), the maximum amount of F^- formed could be 0.36 mg.L^{-1} of F^- . The fluoride concentration has been measured at the end of the total treatment (after 72 h) and the value obtained, 0.48 mg.L^{-1} of F^- , was greater than the maximum expected. This result showed that photolysis reactions have taken place with the adsorbed CIP molecules on the ACF10. Therefore, a partial regeneration of the adsorbent could be possible with UV irradiation.

TOC measurements of the final solution showed 76% carbon removal for ACF10 (final TOC $3.15 \text{ mg}_c.\text{L}^{-1}$). The treatment increased the removal rate from 72% (first adsorption) to 76%. This result is in agreement with the results shown in Figure 6: some aromatic transformation products remained after 3 days of treatment.

With the adsorption/photolysis sequential process, the irradiation step allowed an increase of the CIP removal kinetics, but transformation products remained in the liquid at the end of the treatment. These results show that this type of coupling is of little interest.

3.2.2 The Adsorption and Photocatalysis Coupling Process

Characteristic of the Composite Material. TiO₂ columnar coatings, as shown in Figure 7, were performed on activated superficial carbon fibers via the MOCVD technique. The deposition only occurred on superficial fibers of the ACF10 (on both sides of the fabric) while the internal fibers remained uncoated - the MOCVD setup not allowing growth by chemical vapor infiltration. A significant number of molecules could then be adsorbed on the uncoated fibers.

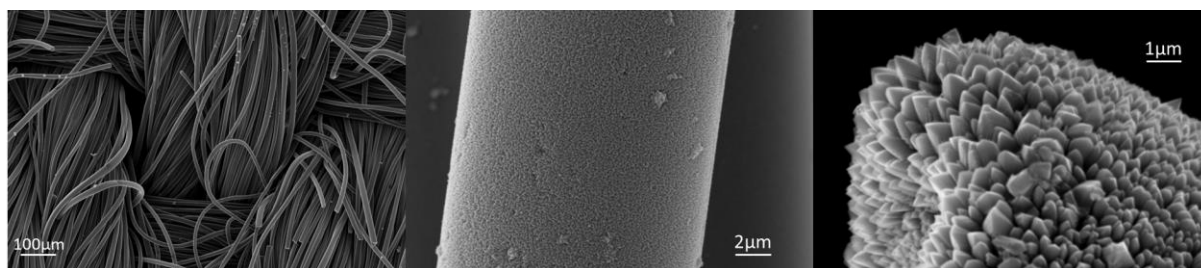


Figure 7 SEM pictures of ACF10 with TiO₂ coating.

The XRD patterns shown in Figure 8 confirm the anatase structure of the TiO₂ coating on the ACF fibers. Concerning ACF, the wide peaks at 23 and 44° are consistent with graphitic carbon structure with a significant dispersion of interreticular distance, allowing us to consider the ACF fibers as being rather amorphous [67].

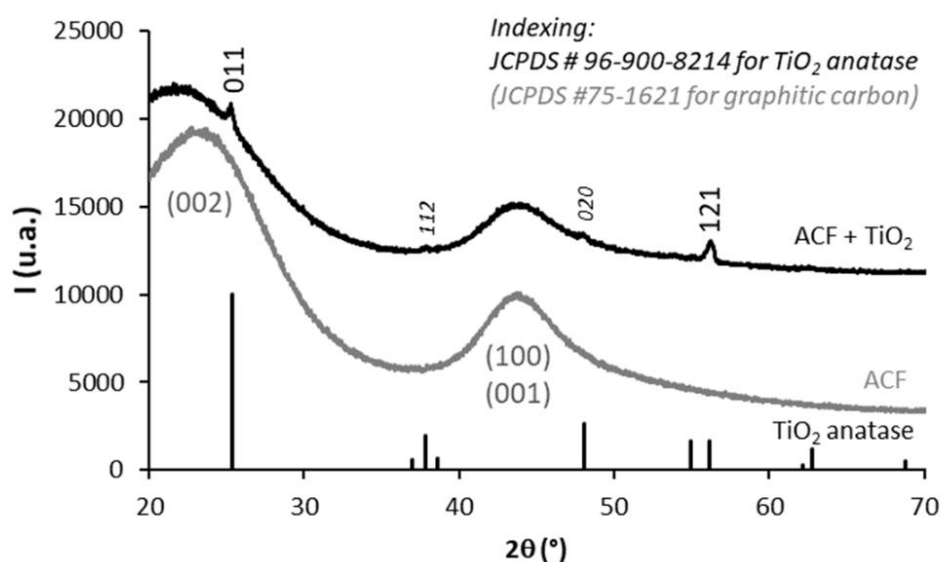


Figure 8 XRD patterns of ACF and ACF-TiO₂.

BET measurements were performed to evaluate the impact of the TiO₂ coating on the physical and adsorption properties of the ACF. Table 7 presents the comparison of the physical characteristics of the two ACFs with and without TiO₂ deposition. The presence of the catalyst has a low impact on the physical characteristics of ACFs in terms of BET surface and pore volume.

Table 7 Comparison of ACF physical characteristics with and without TiO₂ deposition.

ACF	ACF10	
TiO ₂ coating	Without	With
S _{BET} (m ² .g ⁻¹)	926	965
V _{T,porous} (cm ³ .g ⁻¹)	0.38	0.39
V _{μporous} (cm ³ .g ⁻¹)	0.35	0.37
V _{mesoporous} (cm ³ .g ⁻¹)	0.032	0.025

Liquid Phase Monitoring. The kinetics of CIP degradation by coupling adsorption and photocatalysis using the composite material ACF10-TiO₂ was compared to that achieved with the adsorption on ACF10 (without UV), and the adsorption/photolysis process presented previously (Figure 9).

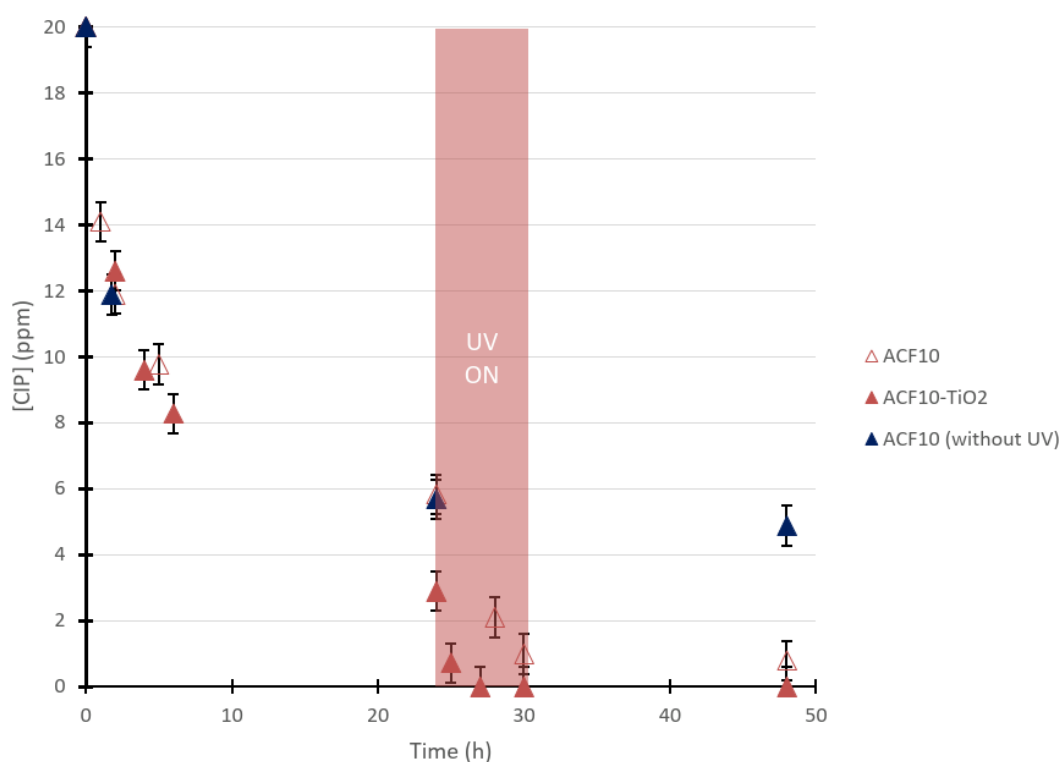


Figure 9 Elimination of ciprofloxacin by coupling adsorption and photocatalysis with ACF-TiO₂ ($C_0 = 20 \text{ mg.L}^{-1}$; $V = 100 \text{ mL}$; $m_{\text{ACF10}} = 193 \text{ mg}$; $I = 10 \text{ mW.cm}^{-2}$; $m_{\text{TiO}_2, \text{coating}} = 3,7 \text{ mg}$; $T = 25 \text{ }^\circ\text{C}$; $Q_v = 200 \text{ mL.min}^{-1}$).

Different adsorption kinetics were observed between ACF10 and ACF10-TiO₂ during the first adsorption step. Faster adsorption was obtained with the composite material, and the adsorbed quantity seems to be higher after 24 h of adsorption: 71% of the CIP was adsorbed by ACF10 without deposited TiO₂, whereas 85% of the CIP was adsorbed by the composite material. Huang et al. (2020) reported a similar behavior with a composite material: CIP adsorbed faster and in greater quantity on straw fibers (adsorbent) having a TiO₂ deposit on its surface [68]. During this first phase of adsorption, the presence of the TiO₂ coating could therefore influence the nature of the interactions as reported by several authors for CIP [68, 69]. The difference between the two adsorption kinetics

could be due to the influence of TiO_2 on the physical properties of the ACF. This deposit can play a role in changing the surface tension of the material and, thus, on its hydrophobicity. Hydrophobicity is known to be a major factor in adsorption kinetics, so a change in surface tension due to the presence of hydrophilic TiO_2 could modify the adsorption kinetics [70]. Moreover, the deposition temperature ($500\text{ }^\circ\text{C}$) can also affect the material. The surface tension of uncoated fibers could be modified by the desorption/degradation of various molecules (residues from manufacturing steps, surrounding atmosphere, etc.) at this temperature. Modification of the properties of the fiber (elasticity and resistance) could also occur, which may reduce external limitations and so increase adsorption kinetics.

Moreover, by using ACF10- TiO_2 , 3 h of irradiation are sufficient to fully eliminate the CIP, whereas, as discussed previously, 6 h of irradiation was not sufficient in the absence of TiO_2 . This result shows that the kinetics of the photocatalytic reactions is much faster than that of photolysis, as already reported by Triquet et al. for CIP [37]. Furthermore, since the concentration in the liquid is lower, faster kinetics is expected as reported for UV adsorption/photocatalysis coupling for the removal of bisphenol A and 2-chlorophenol [71].

As with the adsorption/photolysis coupling, aromatic transformation products were detected using ACF10- TiO_2 (Figure 10). In this process, most of them are completely degraded. The presence of the TiO_2 coating allows, thanks to the action of the UV, the creation of radicals with a strong oxidizing power (OH^\bullet type). These oxidants can rapidly degrade organic molecules in a non-selective way. At the end of the treatment, only two ATPs (F and J) remained in the liquid.

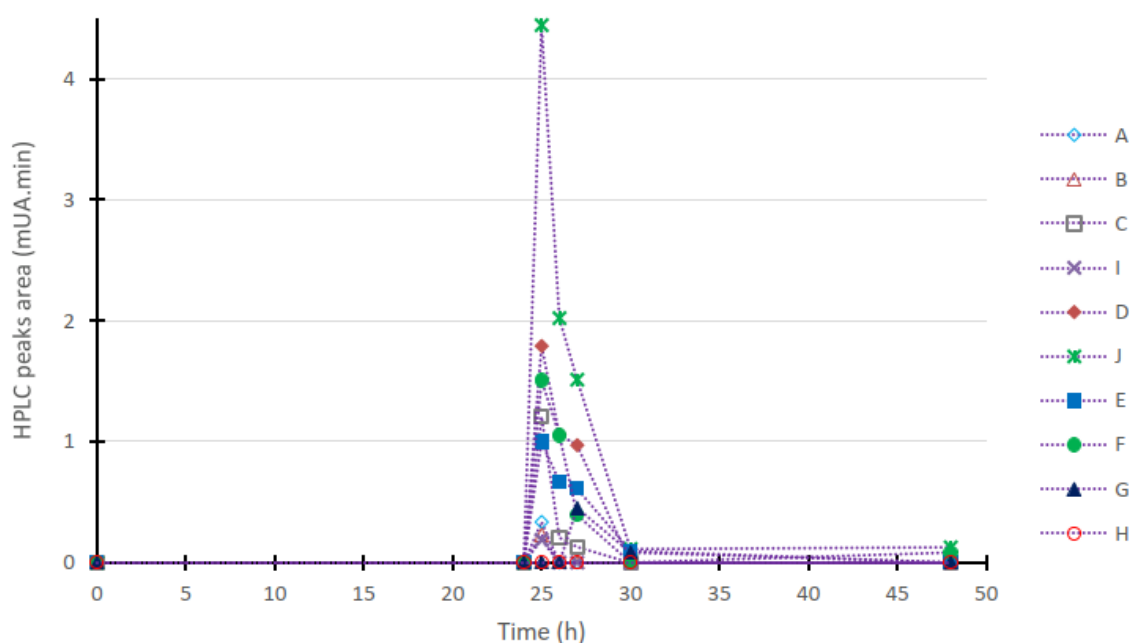


Figure 10 Evolution of ATPs over time for treatment with the ACF10- TiO_2 composite material.

The second indicator of photocatalytic reaction performance is the presence of aliphatic and fluoride in the effluent. At the end of the treatment with the ACF10- TiO_2 , only formic acid has been quantified ($0.70\text{ mg}\cdot\text{L}^{-1}$ of HCOO^-) while oxalic acid $\text{C}_2\text{O}_4^{2-}$ has been just detected. In addition, a pH measurement was performed. An initial pH of 6.8 was recorded. This decreased to 6.3 after 48 h

of treatment. This confirms slight acidification of the effluent and the presence of aliphatic acids. However, such a small difference in pH likely has very little influence on the adsorption and photocatalysis processes. Aliphatics are usually refractory to advanced oxidation processes and are usually detected at the end of this treatment [72]. The fluoride concentration was greater (0.33 mg.L^{-1} of F^-) than expected based on the CIP concentration at the end of the adsorption phase ($[\text{CIP}] = 2.89 \text{ mg.L}^{-1}$; 0.17 mg.L^{-1} of F^- expected). This high amount of fluoride in the solution showed that photochemical reactions took place at the surface of composite material, bringing about its partial regeneration.

Figure 11 shows the evolution of TOC measurements for the different couplings (48 h for adsorption/photocatalysis and 72 h for adsorption/photolysis). For ACF10, the TOC removal rate was 76% for the adsorption/photolysis coupling, whereas it was 89% for the adsorption/photocatalysis. With ACF10-TiO₂, the removal of the CIP is more efficient and more rapid. On the other hand, considering only the adsorption step, the removal rate was 85% (CIP concentration = 2.88 mg.L^{-1}). These values being of the same order of magnitude, it can be concluded that the coupling treatments did not significantly modify the TOC of the solution. The molecules are degraded, but mineralization remained incomplete, and the transformation products (TP) remained in the liquid phase. However, with ACF10-TiO₂, most of the TP were aliphatic acids known to be less toxic, confirming the appeal of this process.

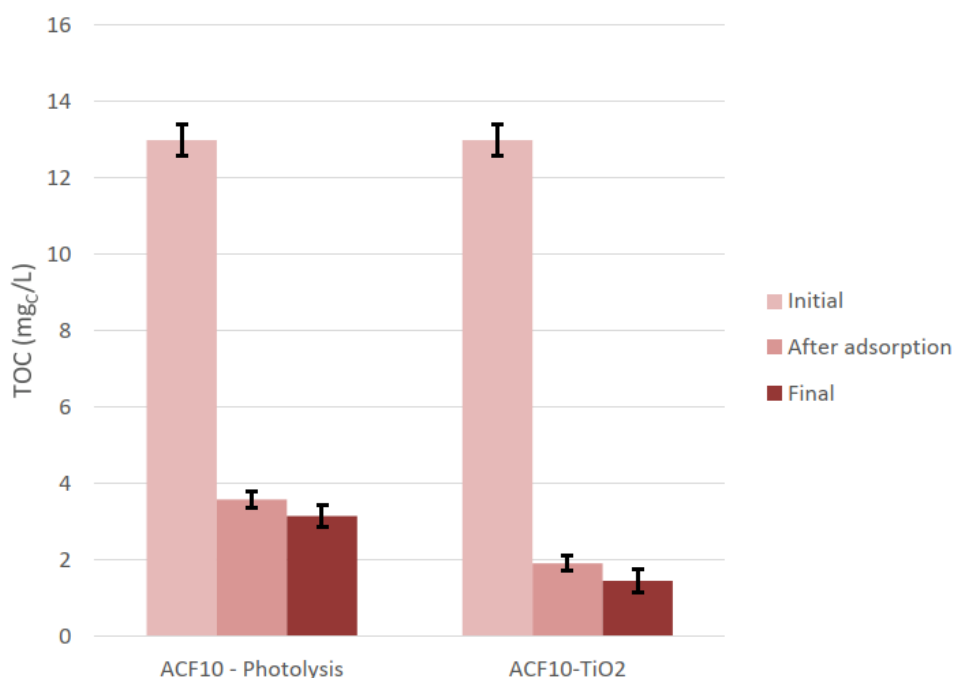


Figure 11 TOC evolution according to the different hybrid processes.

Solid Phase Monitoring. ACF10 and ACF10-TiO₂ were analyzed after 48 h of adsorption/photolysis-photocatalysis experiment by SEM with a backscattered electron detector to highlight chemical contrasts, as well as EDS measurements to confirm the chemical composition.

Figure 12 shows that the deposit survived the 48 h-experiment even if some cracks can be observed. Furthermore, an ICP analysis of the liquid phase showed that very little TiO₂ deposit came off the adsorbent. After the 48 h experiment, less than 0.02 mg of Ti were present in the water (0.5% of initial Ti), which was very low in comparison with the initial Ti mass in the deposit (2.2 mg of Ti in

3.7 mg of TiO_2). Even if the cracking is not significant, a pre-treatment by the acid of the activated carbon fibers could have improved the adsorbent-photocatalyst interactions and, thus, allowed a better adherence of the deposit [73].

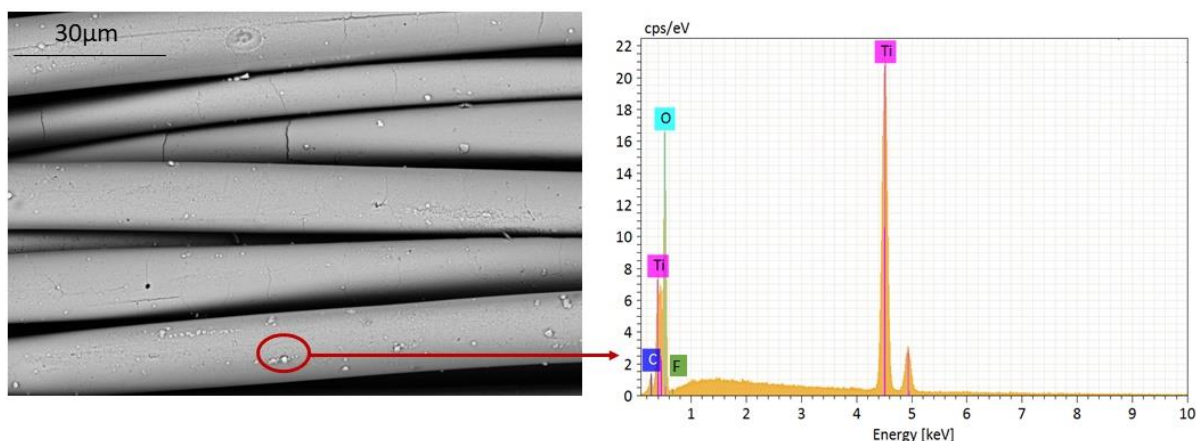


Figure 12 SEM-EDS observation of the ACF10- TiO_2 with a backscattered electron detector after a 48-h adsorption/photocatalysis experiment.

No evidence of adsorbed CIP appears in the EDS graphs of ACF10- TiO_2 - either no CIP remains adsorbed on the TiO_2 , or the fluorine signal is so low that it disappears in the continuum background. In contrast, CIP aggregates were detected on regular ACF10 after the adsorption/photolysis process, as shown in Figure 13.

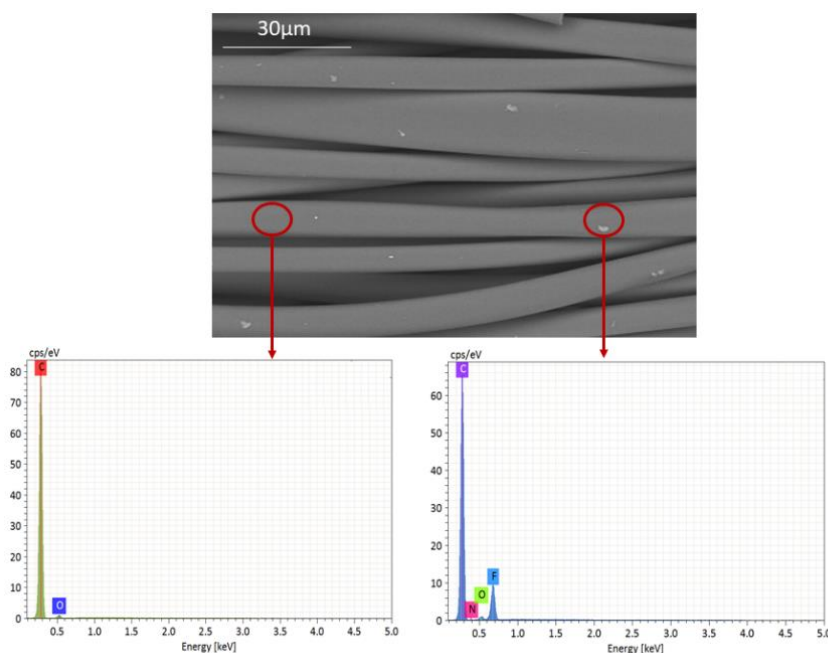


Figure 13 SEM-EDS observation of the ACF10 with a backscattered electron detector after a 48-h adsorption/photolysis experiment.

4. Conclusions

This study investigated a sequential process combining adsorption and photocatalysis for CIP removal. The ACF selected was microporous, with the same range of pore sizes (from 0.5 to 3 nm) but a smaller BET surface area (926 m²/g) than typical ACFs. SEM observations and tensile tests showed that the fibers were little affected by the heat treatment accompanying the TiO₂ deposition step. Moreover, the integrity of the TiO₂ coating was shown to be largely preserved following the adsorption/photocatalysis treatment. The adsorption study demonstrated slow kinetics with only 71% of CIP adsorbed after 24 h (total adsorption after 20 days). The kinetics was successfully fitted with an external diffusion limitation model, confirming the limiting of the external transfer due to the tight weave of the ACF. The sequential adsorption/photocatalysis process with ACF10-TiO₂ presents better performances with a quasi-total elimination of CIP and the aromatic transformation products - only a few aliphatic acids remained in solution. In addition, the large quantity of fluorine found in the solution showed that photo-oxidation reactions happened at the surface of the material. Consequently, it can be concluded that a partial regeneration of the material occurred.

Author Contributions

Conceptualization, TT, CT and CA; methodology, TT, CT and CA; analysis, TT and LL; modelisation, TT; experimentation, TT; writing—original draft preparation, TT, CT, LL, RR and CA; writing—review and editing, TT, CT, LL, RR and CA; supervision, CT and CA; project administration, CT and CA. All authors have read and agreed to the published version of the manuscript.

Competing Interests

The authors have declared that no competing interests exist.

References

1. Thuy HT, Nga LP, Loan TT. Antibiotic contaminants in coastal wetlands from Vietnamese shrimp farming. *Environ Sci Pollut Res*. 2011; 18: 835-841.
2. Tong A, Peake B, Braund R. Disposal practices for unused medications in New Zealand community pharmacies. *J Prim Health Care*. 2011; 3: 197-203.
3. Lage AL, Meireles AM, Marciano AC, Ribeiro JM, de Souza-Fagundes EM, da Silva Martins DC. Ciprofloxacin degradation by first-, second-, and third-generation manganese porphyrins. *J Hazard Mater*. 2018; 360: 445-451.
4. Krzeminski P, Tomei MC, Karaolia P, Langenhoff A, Almeida CM, Felis E, et al. Performance of secondary wastewater treatment methods for the removal of contaminants of emerging concern implicated in crop uptake and antibiotic resistance spread: A review. *Sci Total Environ*. 2019; 648: 1052-1081.
5. Ministry of Ecology, Energy, Sustainable Development and the Sea. Recueil de textes sur l'assainissement [Internet]. Paris: Ministry of Ecology, Energy, Sustainable Development and the Sea; 2009. Available from: <https://dokumen.tips/documents/recueil-de-textes-sur-l-assainissement.html>.

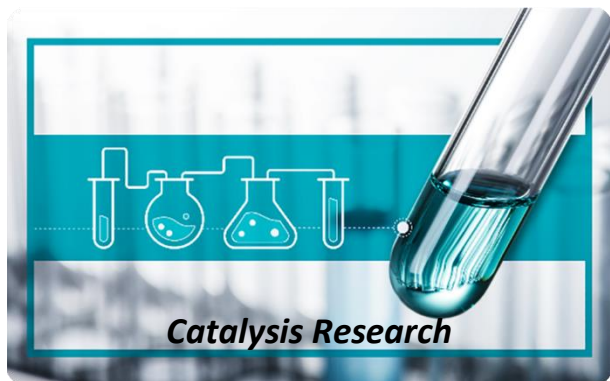
6. González-Hernández Y, Jáuregui-Haza UJ. Improved integrated dynamic model for the simulation of submerged membrane bioreactors for urban and hospital wastewater treatment. *J Membr Sci.* 2021; 624: 119053.
7. Jiuhi QU. Research progress of novel adsorption processes in water purification: A review. *J Environ Sci.* 2008; 20: 1-13.
8. Gupta VK, Ali I. *Environmental water: Advances in treatment, remediation and recycling.* Oxford: Elsevier; 2013.
9. Khan NA, Ahmed S, Farooqi IH, Ali I, Vambol V, Changani F, et al. Occurrence, sources and conventional treatment techniques for various antibiotics present in hospital wastewaters: A critical review. *Trends Analyt Chem.* 2020; 129: 115921.
10. Cárdenas-López C, Camargo G, Giraldo L, Moreno-Piraján JC. Design of an adsorbent employing activated carbon fiber to remove lead. *Eclética Química.* 2007; 32: 61-71.
11. Pignon H, Brasquet C, Le Cloirec P. Coupling ultrafiltration and adsorption onto activated carbon cloth: Application to the treatment of highly coloured wastewaters. *Water Sci Technol.* 2000; 42: 355-362.
12. Chen JY. *Activated carbon fiber and textiles.* Oxford: Woodhead Publishing; 2017.
13. Hassan MF, Sabri MA, Fazal H, Hafeez A, Shezad N, Hussain M. Recent trends in activated carbon fibers production from various precursors and applications-a comparative review. *J Anal Appl Pyrolysis.* 2020; 145: 104715.
14. Wang D, Wang Z, Zheng X, Tian M. Activated carbon fiber derived from the seed hair fibers of *Metaplexis japonica*: Novel efficient adsorbent for methylene blue. *Ind Crops Prod.* 2020; 148: 112319.
15. Li X, Chen S, Fan X, Quan X, Tan F, Zhang Y, et al. Adsorption of ciprofloxacin, bisphenol and 2-chlorophenol on electrospun carbon nanofibers: In comparison with powder activated carbon. *J Colloid Interface Sci.* 2015; 447: 120-127.
16. Srivastava A, Singh M, Karsauliya K, Mondal DP, Khare P, Singh S, et al. Effective elimination of endocrine disrupting bisphenol A and S from drinking water using phenolic resin-based activated carbon fiber: Adsorption, thermodynamic and kinetic studies. *Environ Nanotechnol Monit Manag.* 2020; 14: 100316.
17. Zhao Y, Cho CW, Wang D, Choi JW, Lin S, Yun YS. Simultaneous scavenging of persistent pharmaceuticals with different charges by activated carbon fiber from aqueous environments. *Chemosphere.* 2020; 247: 125909.
18. Wang S, Li X, Zhao H, Quan X, Chen S, Yu H. Enhanced adsorption of ionizable antibiotics on activated carbon fiber under electrochemical assistance in continuous-flow modes. *Water Res.* 2018; 134: 162-169.
19. Whyte HE, Raillard C, Subrenat A, Hequet V. Influence of environmental parameters on the photocatalytic oxidation efficiency of acrylonitrile and isoflurane; two operating room pollutants. *Build Environ.* 2019; 154: 97-106.
20. Paul T, Dodd MC, Strathmann TJ. Photolytic and photocatalytic decomposition of aqueous ciprofloxacin: Transformation products and residual antibacterial activity. *Water Res.* 2010; 44: 3121-3132.
21. Rico-Santacruz M, García-Muñoz P, Keller V, Batail N, Pham C, Robert D, et al. Alveolar TiO₂-β-SiC photocatalytic composite foams with tunable properties for water treatment. *Catal Today.* 2019; 328: 235-242.

22. Ajo P, Preis S, Vornamo T, Mänttari M, Kallioinen M, Louhi-Kultanen M. Hospital wastewater treatment with pilot-scale pulsed corona discharge for removal of pharmaceutical residues. *J Environ Chem Eng.* 2018; 6: 1569-1577.
23. Agustina TE, Ang HM, Vareek VK. A review of synergistic effect of photocatalysis and ozonation on wastewater treatment. *J Photochem Photobiol C.* 2005; 6: 264-273.
24. González Labrada K, Alcorta Cuello DR, Saborit Sánchez I, García Batle M, Manero MH, Barthe L, et al. Optimization of ciprofloxacin degradation in wastewater by homogeneous sono-Fenton process at high frequency. *J Environ Sci Health A.* 2018; 53: 1139-1148.
25. Krishnan RY, Manikandan S, Subbaiya R, Biruntha M, Govarthanam M, Karmegam N. Removal of emerging micropollutants originating from pharmaceuticals and personal care products (PPCPs) in water and wastewater by advanced oxidation processes: A review. *Environ Technol Innov.* 2021; 23: 101757.
26. Matthews RW. Photo-oxidation of organic material in aqueous suspensions of titanium dioxide. *Water Res.* 1986; 20: 569-578.
27. Li S, Hu J. Transformation products formation of ciprofloxacin in UVA/LED and UVA/LED/TiO₂ systems: Impact of natural organic matter characteristics. *Water Res.* 2018; 132: 320-330.
28. Pereira VJ, Galinha J, Crespo MT, Matos CT, Crespo JG. Integration of nanofiltration, UV photolysis, and advanced oxidation processes for the removal of hormones from surface water sources. *Sep Purif Technol.* 2012; 95: 89-96.
29. Lhomme L, Brosillon S, Wolbert D. Photocatalytic degradation of a triazole pesticide, cyproconazole, in water. *J Photochem Photobiol A.* 2007; 188: 34-42.
30. Bettini S, Boutet-Robinet E, Cartier C, Coméra C, Gaultier E, Dupuy J, et al. Food-grade TiO₂ impairs intestinal and systemic immune homeostasis, initiates preneoplastic lesions and promotes aberrant crypt development in the rat colon. *Sci Rep.* 2017; 7: 40373.
31. Dulian P, Nachit W, Jaglarz J, Zięba P, Kanak J, Żukowski W. Photocatalytic methylene blue degradation on multilayer transparent TiO₂ coatings. *Opt Mater.* 2019; 90: 264-272.
32. Schiemann D, Alphonse P, Taberna PL. Synthesis of high surface area TiO₂ coatings on stainless steel by electrophoretic deposition. *J Mater Res.* 2013; 28: 2023-2030.
33. Andriantsiferana C, Mohamed EF, Delmas H. Photocatalytic degradation of an azo-dye on TiO₂/activated carbon composite material. *Environ Technol.* 2014; 35: 355-363.
34. Alalm MG, Tawfik A, Ookawara S. Enhancement of photocatalytic activity of TiO₂ by immobilization on activated carbon for degradation of pharmaceuticals. *J Environ Chem Eng.* 2016; 4: 1929-1937.
35. Tran DT, Mendret J, Méricq JP, Faur C, Brosillon S. Study of permeate flux behavior during photo-filtration using photocatalytic composite membranes. *Chem Eng Process.* 2020; 148: 107781.
36. Ribeiro E, Plantard G, Teyssandier F, Maury F, Sadiki N, Chaumont D, et al. Activated-carbon/TiO₂ composites preparation: An original grafting by milling approach for solar water treatment applications. *J Environ Chem Eng.* 2020; 8: 104115.
37. Triquet T, Tendero C, Latapie L, Manero MH, Richard R, Andriantsiferana C. TiO₂ MOCVD coating for photocatalytic degradation of ciprofloxacin using 365 nm UV LEDs-kinetics and mechanisms. *J Environ Chem Eng.* 2020; 8: 104544.
38. Foo KY, Hameed BH. Decontamination of textile wastewater via TiO₂/activated carbon composite materials. *Adv Colloid Interface Sci.* 2010; 159: 130-143.

39. Tsai JH, Chiang HM, Huang GY, Chiang HL. Adsorption characteristics of acetone, chloroform and acetonitrile on sludge-derived adsorbent, commercial granular activated carbon and activated carbon fibers. *J Hazard Mater.* 2008; 154: 1183-1191.
40. Yue Z, Vakili A, Wang J. Activated carbon fibers from meltblown isotropic pitch fiber webs for vapor phase adsorption of volatile organic compounds. *Chem Eng J.* 2017; 330: 183-190.
41. Lopes FC, Maria da Graça C, Bargiela P, Ferreira HS, Pires CA. Ag/TiO₂ photocatalyst immobilized onto modified natural fibers for photodegradation of anthracene. *Chem Eng Sci.* 2020; 227: 115939.
42. Martínez C, Fernández MI, Santaballa JA, Faria J. Aqueous degradation of diclofenac by heterogeneous photocatalysis using nanostructured materials. *Appl Catal B.* 2011; 107: 110-118.
43. Barakat MA, Kumar R, Eniola JO. Adsorption and photocatalytic scavenging of 2-chlorophenol using carbon nitride-titania nanotubes based nanocomposite: Experimental data, kinetics and mechanism. *Data Brief.* 2021; 34: 106664.
44. Awfa D, Ateia M, Fujii M, Johnson MS, Yoshimura C. Photodegradation of pharmaceuticals and personal care products in water treatment using carbonaceous-TiO₂ composites: A critical review of recent literature. *Water Res.* 2018; 142: 26-45.
45. Wang Y, Chen G, Shen Q, Zhang F, Chen G. Hydrothermal synthesis and photocatalytic activity of combination of flowerlike TiO₂ and activated carbon fibers. *Mater Lett.* 2014; 116: 27-30.
46. Yuan R, Guan R, Shen W, Zheng J. Photocatalytic degradation of methylene blue by a combination of TiO₂ and activated carbon fibers. *J Colloid Interface Sci.* 2005; 282: 87-91.
47. Bai B, Qiu L, Mei D, Jin Z, Song L, Du P. Firmly-supported porous fabric fiber photocatalysts: TiO₂/porous carbon fiber cloth composites and their photocatalytic activity. *Mater Re Bull.* 2022; 148: 111672.
48. Alam U, Pandey K, Verma N. Photocatalytic oxidation of glyphosate and reduction of Cr (VI) in water over ACF-supported CoNiWO₄-gCN composite under batch and flow conditions. *Chemosphere.* 2022; 297: 134119.
49. Jiang ZY, Ma YK, Ke QF, Chu LF, Guo CX, Guo YP. Hydrothermal deposition of CoFe₂O₄ nanoparticles on activated carbon fibers promotes atrazine removal via physical adsorption and photo-Fenton degradation. *J Environ Chem Eng.* 2021; 9: 105940.
50. González-Labrada K, Richard R, Andriantsiferana C, Valdés H, Jáuregui-Haza UJ, Manero MH. Enhancement of ciprofloxacin degradation in aqueous system by heterogeneous catalytic ozonation. *Environ Sci Pollut Res.* 2020; 27: 1246-1255.
51. Caço AI, Varanda F, Pratas de Melo MJ, Dias AM, Dohrn R, Marrucho IM. Solubility of antibiotics in different solvents. Part II. Non-hydrochloride forms of tetracycline and ciprofloxacin. *Ind Eng Chem Res.* 2008; 47: 8083-8089.
52. Sarantopoulos C. Photocatalyseurs à base de TiO₂ préparés par infiltration chimique en phase vapeur (CVI) sur supports microfibreux [Internet]. Toulouse: University of Toulouse; 2007 [cited 2020 February 13th]. Available: <http://ethesis.inp-toulouse.fr/archive/00000545/>.
53. Brunauer S, Emmett PH, Teller E. Adsorption of gases in multimolecular layers. *J Am Chem Soc.* 1938; 60: 309-319.
54. Lastoskie C, Gubbins KE, Quirke N. Pore size distribution analysis of microporous carbons: A density functional theory approach. *J Phys Chem.* 1993; 97: 4786-4796.

55. Seaton NA, Walton JP. A new analysis method for the determination of the pore size distribution of porous carbons from nitrogen adsorption measurements. *Carbon*. 1989; 27: 853-861.
56. Botero-Coy AM, Martínez-Pachón D, Boix C, Rincón RJ, Castillo N, Arias-Marín LP, et al. An investigation into the occurrence and removal of pharmaceuticals in Colombian wastewater. *Sci Total Environ*. 2018; 642: 842-853.
57. Al-Maadheed S, Goktepe I, Latiff AB, Shomar B. Antibiotics in hospital effluent and domestic wastewater treatment plants in Doha, Qatar. *J Water Process Eng*. 2019; 28: 60-68.
58. Morasch B, Bonvin F, Reiser H, Grandjean D, De Alencastro LF, Perazzolo C, et al. Occurrence and fate of micropollutants in the Vidy Bay of Lake Geneva, Switzerland. Part II: Micropollutant removal between wastewater and raw drinking water. *Environ Toxicol Chem*. 2010; 29: 1658-1668.
59. Ruthven DM. Principles of adsorption and adsorption processes. New York: John Wiley & Sons; 1984.
60. Furusawa T, Smith JM. Diffusivities from dynamic adsorption data. *AIChE J*. 1973; 19: 401-403.
61. Weber Jr WJ, Morris JC. Kinetics of adsorption on carbon from solution. *J Sanit Eng Div*. 1963; 89: 31-59.
62. Lagergren SK. About the theory of so-called adsorption of soluble substances. *Sven Vetenskapsakad Handlingar*. 1898; 24: 1-39.
63. Ho YS, McKay G. Pseudo-second order model for sorption processes. *Process Biochem*. 1999; 34: 451-465.
64. Rudzinski W, Plazinski W. Kinetics of solute adsorption at solid/solution interfaces: A theoretical development of the empirical pseudo-first and pseudo-second order kinetic rate equations, based on applying the statistical rate theory of interfacial transport. *J Phys Chem B*. 2006; 110: 16514-16525.
65. Fu P, Luan Y, Dai X. Preparation of activated carbon fibers supported TiO₂ photocatalyst and evaluation of its photocatalytic reactivity. *J Mol Catal A Chem*. 2004; 221: 81-88.
66. Speight JG. Redox Transformations. In: *Reaction mechanisms in environmental engineering*. Oxford: Butterworth-Heinemann; 2018.
67. Descamps M. Etats amorphe et vitreux des composés moléculaires et pharmaceutiques- Propriétés générale [Internet]. Paris: Techniques de l'Ingénieur; 2017. Available from: <https://www.techniques-ingenieur.fr/base-documentaire/biomedical-pharma-th15/mise-en-forme-des-medicaments-et-autres-produits-de-sante-42611210/etats-amorphe-et-vitreux-des-composes-moleculaires-et-pharmaceutiques-pha2030/>.
68. Huang X, Wu S, Tang S, Huang L, Zhu D, Hu Q. Photocatalytic hydrogel layer supported on alkali modified straw fibers for ciprofloxacin removal from water. *J Mol Liq*. 2020; 317: 113961.
69. Tan XF, Liu YG, Gu YL, Xu Y, Zeng GM, Hu XJ, et al. Biochar-based nano-composites for the decontamination of wastewater: A review. *Bioresour Technol*. 2016; 212: 318-333.
70. Moreno-Castilla C., Adsorption of organic molecules from aqueous solutions on carbon materials. *Carbon*. 2004; 42: 83-94
71. Nguyen TD, Jitae K, Viet NM, Thang PQ, Huong PT. Combination of La-TiO₂ and activated carbon fiber for degradation of toxic organic pollutants under the visible light. *J Environ Chem Eng*. 2019; 7: 103180.

72. Wang XS, Song H, Zhang J, Liu YL, Ma J, Wang L. Chlorination decreases acute toxicity of iodophenols through the formation of iodate and chlorinated aliphatic disinfection byproducts. *Water Res.* 2021; 194: 116951.
73. Lei L, Wang W, Wang C, Zhang M, Zhong Q, Fan H. In situ growth of boron doped g-C₃N₄ on carbon fiber cloth as a recycled flexible film-photocatalyst. *Ceram Int.* 2021; 47: 1258-1267.



Enjoy *Catalysis Research* by:

1. [Submitting a manuscript](#)
2. [Joining in volunteer reviewer bank](#)
3. [Joining Editorial Board](#)
4. [Guest editing a special issue](#)

For more details, please visit:

<http://www.lidsen.com/journals/cr>